

# Multiple stellar populations in the globular cluster M3 (NGC 5272): a Strömgren perspective

Davide Massari,<sup>1,2\*</sup> Emilio Lapenna,<sup>3,1</sup> Angela Bragaglia,<sup>1</sup> Emanuele Dalessandro,<sup>3</sup> Rodrigo Contreras Ramos,<sup>4,5</sup> Pía Amigo<sup>4,5</sup>

<sup>1</sup>INAF-Osservatorio Astronomico di Bologna, via Ranzani 1, I–40127, Bologna, Italy

<sup>2</sup>University of Groningen, Kapteyn Astron Institute, NL-9747 AD Groningen, Netherlands

<sup>3</sup>Dipartimento di Fisica e Astronomia, Università degli Studi di Bologna, v.le Bertoni Pichat 6/2, I–40127 Bologna, Italy

<sup>4</sup>Millennium Institute of Astrophysics, Av. Vicua Mackenna 4860, 782-0436 Macul, Santiago, Chile

<sup>5</sup>Instituto de Astrofísica, Pontificia Universidad Católica de Chile, Av. Vicua Mackenna 4860, 782-0436 Macul, Chile

Accepted 2016 March 8. Received 2016 March 4; in original form 2016 February 10

## ABSTRACT

We present Strömgren photometry of the Galactic Globular Cluster M3 to study its multiple generations phenomenon. The use of different colour-magnitude diagrams and especially of the notoriously efficient  $c_y$  index allowed us to detect a double Red Giant Branch in the cluster CMD. After decontamination from fore- and background sources, the two sequences turned out to be equally populated. The two components also show a bimodal radial distribution well corresponding to that predicted by numerical simulations for clusters living in an intermediate dynamical evolutive state and with a population with modified chemical composition that was born more centrally concentrated than the primordial. The analysis of high-resolution spectra quantitatively demonstrates that the two detected sequences correspond to the first (Na-poor) generation and the second (Na-rich) generation, thus confirming the importance of synergy between photometry and spectroscopy.

**Key words:** Hertzsprung-Russell and colour-magnitude diagrams - stars: Population II - stars: abundances techniques: photometric globular clusters: general

## 1 INTRODUCTION

Galactic Globular Clusters (GCs) had been considered the best example of simple stellar population (e.g., [Renzini & Buzzoni 1986](#)). However, in the last decades strong observational evidence has been gathered to prove that this is only a first approximation. In fact, GCs host multiple populations of stars differing in terms of chemical composition (for a recent review see [Gratton, Carretta, & Bragaglia 2012](#)) which also reflects in spreads and splits of the evolutionary sequences in colour-magnitude diagrams (CMDs, see e.g., [Monelli et al. 2013](#); [Piotto et al. 2015](#)).

The multiple population phenomenon is very complex and not totally understood yet (see [Salaris & Cassisi 2014](#); [Bastian, Cabrera-Ziri, & Salaris 2015a](#); [Renzini et al. 2015](#)). The most common chemical signature of GCs is the star-to-star dispersion in light elements (C, N, O, Na, Mg, Al), showing anti-correlations and bi- or multi-modality (see [Gratton, Carretta, & Bragaglia \(2012\)](#)). All the massive Milky Way GCs studied so far,<sup>1</sup> show the Na-O anti-correlation (see

[Carretta et al. 2009a](#) for an extensive database, [Bragaglia et al. 2015](#) and references therein) and some of them also show a Mg-Al anti-correlation (e.g., [Carretta et al. 2009b](#); [Mészáros et al. 2015](#)). Up to now, a sub-sample of properly studied (see [Bastian, Cabrera-Ziri, & Salaris 2015b](#) and references therein) show evidence of internal helium variation, with extreme cases being  $\omega$ -Centauri ([Bedin et al. 2004](#); [Piotto et al. 2005](#); [Dupree & Avrett 2013](#)) and NGC 2808 ([D’Antona et al. 2005](#); [Piotto et al. 2007](#); [Dalessandro et al. 2011](#); [Pasquini et al. 2011](#); [Milone et al. 2015](#); [Massari et al. 2016](#)).

Much less common is instead an internal dispersion in iron content, often combined with a dispersion in neutron-capture elements. Apart from the extreme cases of  $\omega$  Cen ([Norris & Da Costa 1995](#); [Lee et al. 1999](#); [Johnson & Pilachowski 2010](#); [Marino et al. 2011b](#)) and Terzan 5 ([Ferraro et al. 2009](#); [Origlia et al. 2011, 2013](#); [Massari et al. 2014a](#)), with variation larger than 1 dex, several other clusters show variations of (some) 0.1 dex at most. M54

the Sgr dSph, shows a hint of Na enhancement in a minority of stars ([Carretta et al. 2014](#)), while Terzan 7 and Pal 12, another two Sgr clusters, do not show anti-correlations, albeit on very small samples ([Sbordone et al. 2004](#); [Tautvaišienė et al. 2004](#); [Cohen 2004](#)).

\* E-mail: [davide.massari@oabo.inaf.it](mailto:davide.massari@oabo.inaf.it)

<sup>1</sup> The only exception to date is Ruprecht 106 ([Villanova et al. 2013](#)), which is massive and relatively young. Terzan 8, a GC belonging to

(Carretta et al. 2010b), M19 (Johnson et al. 2015a) NGC 5286 (Marino et al. 2015) and M2 (Yong et al. 2014; Milone et al. 2015, but see also Lardo, Mucciarelli, & Bastian 2016 who found the cluster to have only a very small iron-enriched population) belong to this class of object. For other clusters like M22 (Marino et al. 2011a; Mucciarelli et al. 2015a), NGC3201 (Mucciarelli et al. 2015b) and NGC1851 (Carretta et al. 2011a; Yong & Grundahl 2008) the existence of an intrinsic iron spread is still a matter of debate. Since a spread in the iron content might only be explained in terms of supernovae ejecta self-enrichment, for all these clusters a peculiar origin is usually invoked.

Photometric studies showed that the GC multiple population phenomenon (in the following, we will refer to the terms population and generation without distinction, since it is beyond the aim of this paper to favour multiple population scenarios which support multiple episode of star formation as in Decressin et al. 2007; D’Ercole et al. 2008, or which do not, see Bastian et al. 2013) can be addressed in detail using a proper combination of filters (see e.g. Han et al. 2009; Carretta et al. 2011b; Milone et al. 2012; Monelli et al. 2013). In this sense, one of the best way to study the multiple populations of GCs comes from medium-band Strömgren *uvby* photometry. In fact the *u* and *v* filters of this set cover the spectral region including the NH and CN molecular bands at 3400Å and 4316Å, respectively, and they are therefore sensitive to variations in the C and N abundances. The proof of the efficiency of Strömgren photometry for this kind of study comes from both observational and theoretical works such as Yong et al. (2008); Carretta et al. (2011b); Sbordone et al. (2011); Roh et al. (2011), where the authors built suitable combination of filters to enhance the separation among multiple RGB sequences.

In this paper, we focus our attention on the GC M3 (NGC 5272). M3 is a northern, metal-poor GC, with a metallicity of about  $[Fe/H] \simeq -1.5$  dex (Harris 1996, 2010 edition), which shows evidence of variation in Na, O, Mg and Al (Snedden et al. 2004; Johnson et al. 2005; Cohen & Meléndez 2005; Mészáros et al. 2015). Moreover, the analysis of its HB morphology performed in Dalessandro et al. (2013) by using HST photometry inferred an internal helium spread of  $\Delta Y \simeq 0.02$ . This result has been recently qualitatively confirmed by Valcarce et al. (2016) using Strömgren photometry. Until now, no high-precision photometric studies have been dedicated to the search and analysis of multiple populations in this cluster. Only a rough evidence for an anomalous spread of its RGB colour distribution was found by Lardo et al. (2011) using Sloan photometry, while Piotto et al. (2015) simply showed the existence of a double RGB in the cluster CMD coming from the HST UV Legacy Survey of Galactic GC, postponing the analysis to future papers. For these reasons we exploited deep images taken with Strömgren *uvby* filters to provide a complete study of the multiple generations of stars in M3 and complemented it with the analysis of high-resolution spectra. Strömgren photometry for M3 has been already used by Grundahl et al. (1999). However, this photometry is not publicly available and has furthermore been acquired on a small field of view ( $3.8 \times 3.8$  arcmin<sup>2</sup>, with the NOT). Our study covers a much larger field of view and we will make the catalogue available through the CDS<sup>2</sup>.

The paper is organized as follows. In Sect.2 we provide all the details on the photometric dataset and its reduction, while in Sect.3 we present the results coming from such an analysis. In Sect.4 the complementary spectroscopic analysis is described and the results

**Table 1.** Photometric dataset.

Filter	$t_{exp}$ [s]	$n_{exp}$
<i>u</i>	60	5
	180	4
	500	1
<i>v</i>	60	4
	180	3
<i>b</i>	10	8
	15	1
	20	1
	60	5
	180	2
<i>y</i>	20	2
	60	5
	180	2

obtained from the comparison of the two investigations are shown in Sect.5. Finally, we draw our conclusions in Sect.6.

## 2 PHOTOMETRIC DATA AND ANALYSIS

The photometric dataset analysed in this work consists of a large sample of archival images obtained with the Isaac Newton Telescope - Wide Field Camera (INT-WFC) in medium-band Strömgren filters. The INT-WFC detector consists of four chips, with a pixel scale of  $0.33'' \text{ pixel}^{-1}$ . Each chip covers an area of  $23.1' \times 12.1'$  and they describe a structured field of view where intra-chip gaps are about  $1'$  wide, as shown in Fig.1.

The retrieved archival observations belong to different datasets and cover several nights, from the 22nd of March 2001 to the 9th of May 2006. During these nights several dithered exposures of M3 have been taken in the *u*, *v*, *b*, *y* Strömgren filters. Tab.1 summarises the entire dataset, listing the filters used, exposure times and the total number of exposures analysed.

The pre-reduction of the raw images has been performed by means of standard procedures and the use of the IRAF<sup>3</sup> package, treating each chip of each exposure separately. For each chip and filter, we retrieved from the Isaac Newton Group-ING archive 25 bias and 20 flat-field frames per filter, observed during the analysed observing runs. We used these samples to compute 3 sigma-clipped median bias and flat-field images by means of the *zerocombine* and *flatcombine* IRAF tasks. The final scientific images have been obtained using the *ccdproc* IRAF task.

The photometric reduction has been performed by means of DAOPHOT and ALLSTAR (Stetson 1987) and refined using ALLFRAME (Stetson 1994). In the latter step we used as input for ALLFRAME a catalogue of all the sources found in at least three *b*-band images, since they were those with the larger number of detections. After these steps, for each chip and filter we built a catalogue by requiring that each star fell in at least two of the reduced single exposures. Since for each filter at least two short exposures exist, this choice allowed us to always recover also the brightest stars that saturate in the long exposures. We built a multi-wavelength catalogue

<sup>3</sup> IRAF is distributed by the National Optical Astronomy Observatory, which is operated by the Association of Universities for Research in Astronomy, Inc., under cooperative agreement with the National Science Foundation

<sup>2</sup> <http://cdsweb.u-strasbg.fr>

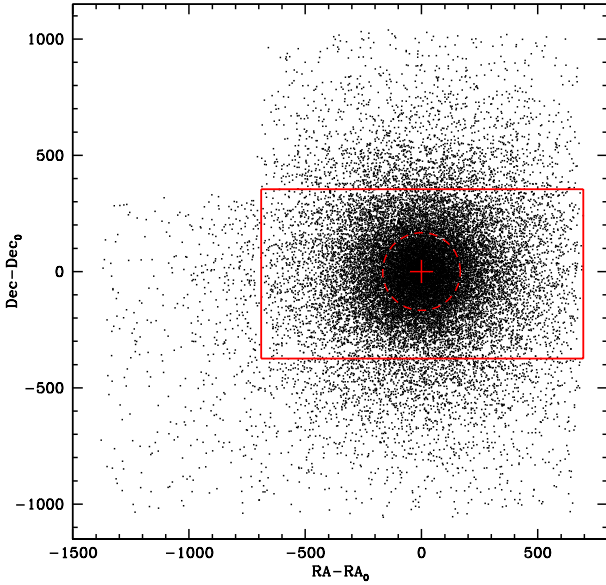


**Figure 1.** Map of the sources detected in our photometric catalogue. The centre of the cluster (Miocchi et al. 2013) is marked with a red cross. The size of chip 4, which is used throughout the analysis, is also delimited with a red box.

for each chip by matching the single-filter catalogues and including all the stars with at least two measured Strömgren magnitudes. Finally, for each single-chip catalogue we transformed stellar positions onto the 2MASS astrometric system (Skrutskie et al. 2006) by using the CataPack software written by P. Montegriffo<sup>4</sup> and after calibrating their magnitudes we merged them together to build the final catalogue. The calibration onto the Strömgren system has been achieved using ten standard stars observed during the night of the 22nd of March 2001. Their calibrated magnitudes in the  $uvby$  filters have been taken from the catalogue of Paunzen (2015).

The spatial distribution of the sources that we recovered through our photometric analysis is shown in Fig.1, where all the stars are plotted as black dots. The centre of the cluster ( $RA_0 = 13:42:11.38$ ,  $Dec_0 = +28:22:39.1$  from Miocchi et al. 2013) is marked as reference with a red cross, while the red circle describes the cluster half-mass radius ( $r_{hm} \sim 167''$ , see Miocchi et al. 2013).

The aim of our work is to study the multiple stellar generations of M3. This requires high precision in terms of photometric uncertainties. All the photometric standards have been observed only with the central chip 4 of the INT camera, and since only few stars are in common among the adjacent chips, we decided to focus the following analysis only on chip 4 itself. In this way, the uncertainties coming from the calibration procedure among the four chips are avoided, and the covered field of view (see the red box in Fig.1) is still sufficiently large to grant a good statistic in terms of detection. In fact, within the central chip fall 17155 sources, which correspond to the 79% of the whole sample of sources detected considering the entire camera. Moreover, the selected chip samples the central regions of M3 out to  $\sim 760''$ , that is more than 4.5 times the cluster  $r_{hm}$ .

<sup>4</sup> [www.bo.astro.it/~paolo/Main/CataPack.html](http://www.bo.astro.it/~paolo/Main/CataPack.html)

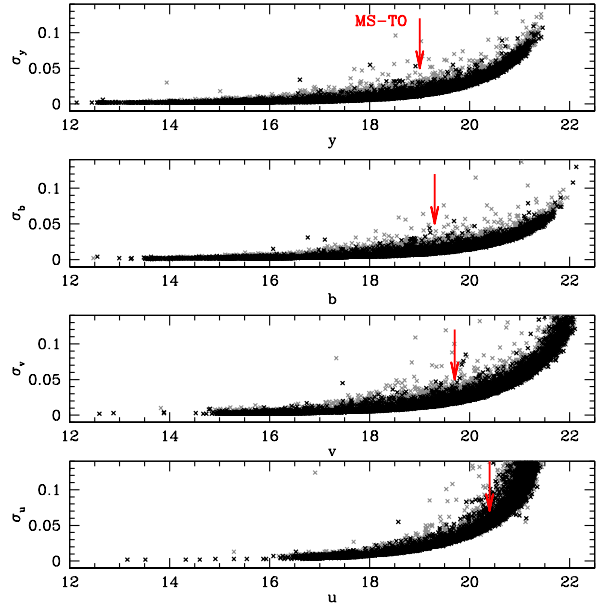


**Figure 2.** Photometric uncertainties for all the four Strömgren filters used as a function of the corresponding magnitude. Stars with  $|sh| > 0.2$  are plotted as grey dots. The location in magnitude of the cluster Main-Sequence Turn-Off is marked with a red arrow.

### 3 STRÖMGREN CMDS

The four panels of Fig.2 show the behaviour of the photometric errors  $\sigma$ , defined as the standard deviation of each star magnitude around the mean of the single-exposure measurements, as a function of the observed magnitudes. The scale of the plots has been kept fixed in order to show that in all filters, magnitudes brighter than the Main Sequence Turn Off (MS-TO, marked in the Figure with red arrows) have internal uncertainties smaller than 0.03 mag, the only exception being the u-band, where the median error at the MS-TO level is 0.05 mag. The  $(y, b - y)$  CMD of M3 is shown in the left panel of Fig.3. All the evolutionary sequences appear to be very well defined, from a few magnitudes below the MS-TO to the RGB-tip, where stars saturate at  $y < 12.7$  mag. The same features are clearly visible in the  $(y, v - y)$  CMD (right panel of Fig.3), which covers a much wider colour baseline. A qualitative comparison with photometry presented in Grundahl et al. (1999) reveals no significant differences both in terms of the RGB extent and HB morphology.

As shown in several previous works, a proper combination of Strömgren filters can unveil the presence of chemical anomalies in GC stellar populations. The index  $m_1$  (defined as  $m_1 = (v - b) - (b - y)$ , Richter, Hilker, & Richtler 1999) is sensible to the cluster metallicity. Left panel of Fig.4 shows the  $(y, m_1)$  CMD of M3. In this case, the spread of such index is  $\sigma_{m_1} = 0.06$  mag at  $16 < y < 16.5$ , consistent with the photometric errors in this magnitude range and thus suggesting that M3 is homogeneous in terms of global metallicity. On the other hand, the index  $\delta_4 = (u - v) - (b - y)$  (Carretta et al. 2011b) is able to reveal the presence of chemical anomalies in the light element abundances of all the GCs studied so far, regardless of their global metal content. The right panel of Fig.4 shows the cluster  $(y, \delta_4)$  CMD. The spread of  $\delta_4$  at the same magnitude interval as before is  $\sigma_{\delta_4} = 0.08$  mag, larger than  $\sigma_{m_1}$ . Since such a value cannot be ascribed to

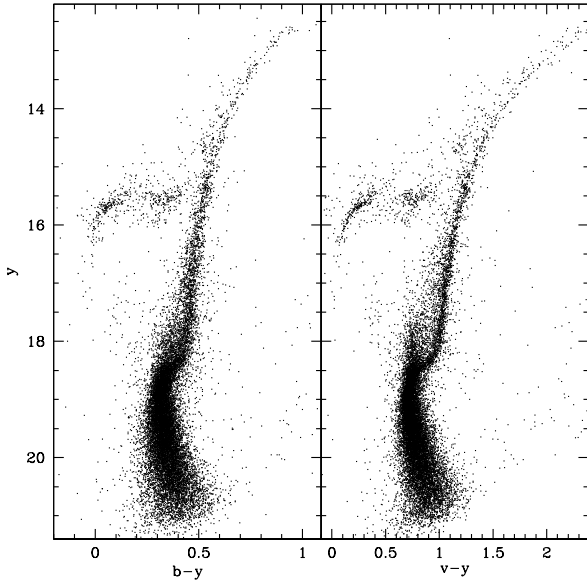


**Figure 3.**  $(y, b - y)$  and  $(y, v - y)$  CMDs of M3.

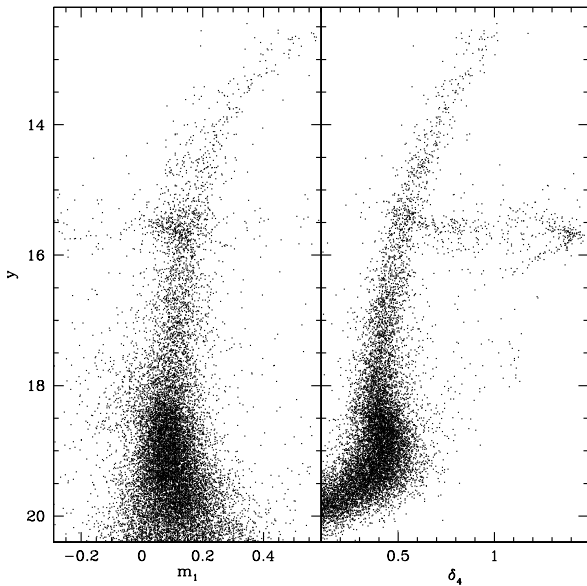


**Figure 4.**  $(y, m_1)$  and  $(y, \delta_4)$  CMD of M3.

larger photometric errors coming from the introduction of the  $u$ -band (that at the RGB level has uncertainties very similar to those measured for the other bands, see Fig.2) in the index, we interpret it as suggestive of an intrinsic spread.

Anthony-Twarog, Twarog, & Craig (1995) used the index  $c_1 = (u - v) - (v - b)$ , which is sensible to the strength of CN and CH bands. This colour index has been subsequently used for example by Grundahl, VandenBerg, & Andersen (1998) to study the chemical anomalies in the stellar population of M13 or by Yong et al. (2008) for NGC 6752. The last authors also defined another index called  $c_y = (c_1) - (b - y)$ , which is still sensitive

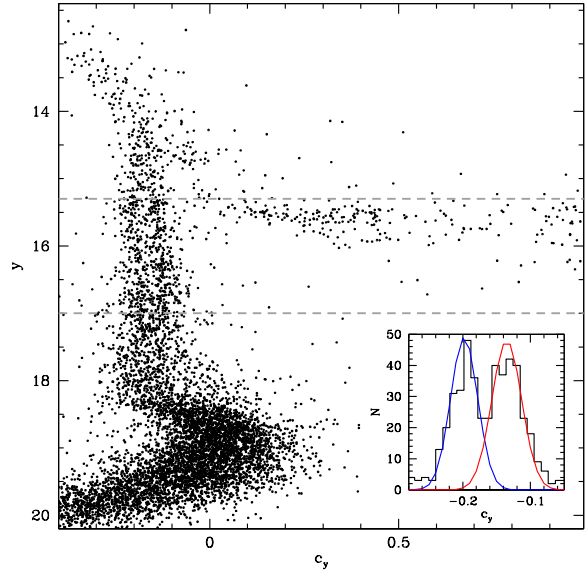


**Figure 5.**  $c_y, y$  CMD for stars with sharpness values  $-0.2 < sh < 0.2$ . The RGB clearly splits in two separated sequences. *Inset:* histogram of the colour distribution of stars in the RGB magnitude interval  $15.3 < y < 17$ .

to  $N$  but insensitive to temperature, and which has been extensively used to distinguish between first generation (FG) and second generation (SG) stars, being well correlated with Na abundances (see e.g. Carretta et al. 2009a). An extensive theoretical study on the influence of the typical chemical anomalies observed in GCs on the behaviour of stellar sequences in Strömgren CMDs has been presented in Sbordone et al. (2011), while Carretta et al. (2011b) approached the problem from the observational side. According to both theoretical and observational findings (see Fig.13 in Carretta et al. 2011b to see the expected differences for stars N-rich and N-poor in different evolutionary phases and of different metallicity),  $c_y$  appears to be the most efficient index to study the multiple populations in M3 (which has a metallicity of about  $[Fe/H] \sim -1.5$  dex).

Fig.5 shows the  $(y, c_y)$  CMD, obtained after excluding all the sources with a sharpness parameter (defined by DAOPHOT as a shape-parameter whose value is zero for perfectly round and point-like sources as expected for stars)  $|sh| > 0.2$ . They are also shown as grey dots in Fig.2.

As immediately evident, in this combination of filters the RGB of M3 splits in two separated sequences. The inset highlights the colour distribution of RGB stars in the magnitude range  $15.3 < y < 17$ , where the separation appears clearer. Such a distribution clearly displays two peaks, separated by about 0.05 mag. According to Carretta et al. (2011b), the left sequence should be populated by N-poor, Na-poor FG stars, while the right sequence by N-rich, Na-rich SG stars. Looking at their Figs. 1 and 2, we note that such a clear bimodal distribution seems rather unusual. The only case resembling M3 is NGC 288, a slightly metal-richer and less massive GC. While the different level of  $N$  is demonstrated by photometry, we will come back on Na in Sections 4 and 5. To test the statistical significance of this bimodality, we performed a GMM test (Muratov & Gnedin 2010), which confirmed that the unimodal hypothesis has to be rejected with a probability larger than 99.99%. Such a result is confirmed independently

also by a dip-test. The GMM test also gives as output the probability for each star to belong to one of the two components. We assigned each star to FG or SG (blue and red dots in Figure 6, respectively) according to their membership probability. In this way the right component accounts for 309 stars, that is the  $52 \pm 3\%$ , while the left component is made up of 283 stars, corresponding to the  $48 \pm 3\%$ . Such an equal (within the uncertainty) distribution between FG and SG is quite rare among Galactic GCs and to date it has been observed only in NGC 6362 (see Dalessandro et al. 2014) and NGC 288 (Carretta et al. 2011b) for which however there is some discrepancy between population ratios based on photometry and on spectroscopy (Carretta et al. 2009a). Also NGC 2808 has an almost equal fraction of FG and SG stars, but this cluster presents more extreme behaviour and has recently been attributed no less than five separate populations (Milone et al. 2015; Carretta 2015).

### 3.1 Radial distribution

The radial distribution of multiple populations in GCs provides important information regarding their origin and formation (Vesperini et al. 2013; Dalessandro et al. 2014; Larsen et al. 2015). According to the theoretical scenarios proposed so far, the second population(s) formed from the polluting material ejected by the primordial one should form in the central regions of a GC, thus appearing more centrally concentrated (see e.g. Decressin et al. 2007; D’Ercole et al. 2008; Bastian, Cabrera-Ziri, & Salaris 2015b). So far, most of the observations (e.g. Carretta et al. 2009b; Lardo et al. 2011; Beccari et al. 2013) have confirmed this prediction. Few notable exceptions have been recently found, such as NGC6362 (Dalessandro et al. 2014) and NGC6121 (Nardiello et al. 2015), which do not show significant radial differences at any distance from the cluster centres. This observational evidence can be interpreted as the effect of an efficient dynamical evolution possibly connected with a significant stellar mass loss (Vesperini et al. 2013; Dalessandro et al. 2014; Miholics, Webb, & Sills 2015). Another unique case so far is represented by M15 (Larsen et al. 2015), in which FG stars appear to be more centrally concentrated than SG ones. The authors suggest that this is due to peculiar initial conditions, however alternative explanations have been recently proposed (Henault-Brunet 2015).

To study the radial distribution of multiple populations in M3, we focus on the RGB only. As a first step, following the method described in Frank et al. (2015), we decontaminated the samples of FG and SG RGB stars described in Sect.3 using a proper selection in the  $b - y, c_1$  and  $b - y, m_1$  planes. The insets of Fig.6 show the criteria adopted for such a selection. In the upper inset, we included in the  $b - y, c_1$  all the sources with  $c_1 < 0.2$  mag (see Árnadóttir, Feltzing, & Lundström 2010), while in the lower inset we kept only stars running parallel to the iso-metallicity line of the cluster RGB (see Calamida et al. 2007), within  $\pm 3\sigma$  from the best-fitting line. After this procedure, 36 stars in the previously described magnitude interval ( $15.3 < y < 17$ ) were discarded, but the SG-to-FG ratio remained unchanged.

At this point, in Fig.7 we plot the radial distributions of the two decontaminated stellar generations. Overall, the trend observed for the red sequence is different from the other, as demonstrated by a Kolmogorov-Smirnov (KS) test which gives a probability  $P > 99.8\%$  that the two distributions are not extracted from the same population. However, at a closer look this overall trend can be divided in three separated intervals. Within the innermost  $95''$  (i.e.  $\sim 0.6$  cluster  $r_{hm}$ , see Mocchi et al. 2013), the two radial distributions appear very similar (the KS test gives a probability of being

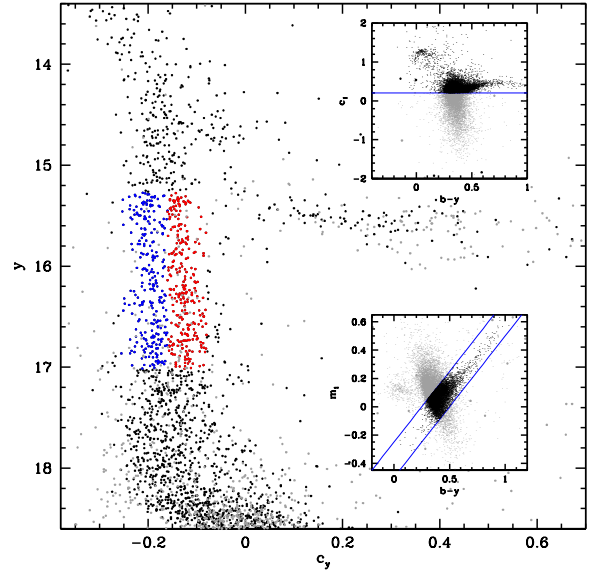


**Figure 6.** Decontaminated RGB of M3 (black dots) in the  $c_y, y$  CMD. The selection criteria are shown in the two inset, where we followed the prescriptions in (Frank et al. 2015) using the  $b - y, c_1$  and  $b - y, m_1$  planes.

identical larger than 94%) and no gradient is found in the trend of SG-to-FG ratio against distance from the cluster centre (see first two points at 0.2 and 0.6  $r_{hm}$  in the bottom panel of Fig.7). On the other hand, outside  $\sim 0.6 r_{hm}$ , the FG stars become progressively less concentrated but more numerous, and the relative number ratio reaches a minimum at  $\sim 2 r_{hm}$ . At that point, the trend inverts and the SG-to-FG ratio reaches a value similar to that observed in the cluster central regions. The final overall trend therefore describes a bimodal behaviour and shows that the two populations are numerically similar only globally, but not locally.

This result demonstrates that it is crucial to cover the entire extent or a significant portion of a stellar cluster to properly study the radial distribution of its multiple populations.

The SG-to-FG radial profile of M3 has been previously studied also by Lardo et al. (2011) based on Sloan photometry. Their sample did not cover the innermost regions of the cluster due to stellar crowding, and their analysis starts at  $r > 100''$ , where the two distributions appear to agree with our findings. This peculiar bimodal profile resembles very well the prediction of Vesperini et al. (2013) for a cluster with an initially more concentrated SG and which underwent intermediate dynamical evolution (see their Figure 7). In this particular case, the mixing of the two generations has started in the innermost regions, where the relaxation time is shorter due to the larger number of interacting stars, but has not reached the entire cluster extent yet, as it happens in the most dynamically evolved clusters (see Dalessandro et al. 2014). Such a dynamical state is also independently confirmed by the radial distribution of Blue Straggler Stars, that in the dynamical clock framework described by Ferraro et al. (2012) places this cluster among their Family-II sample (i.e. systems with intermediate dynamical age).

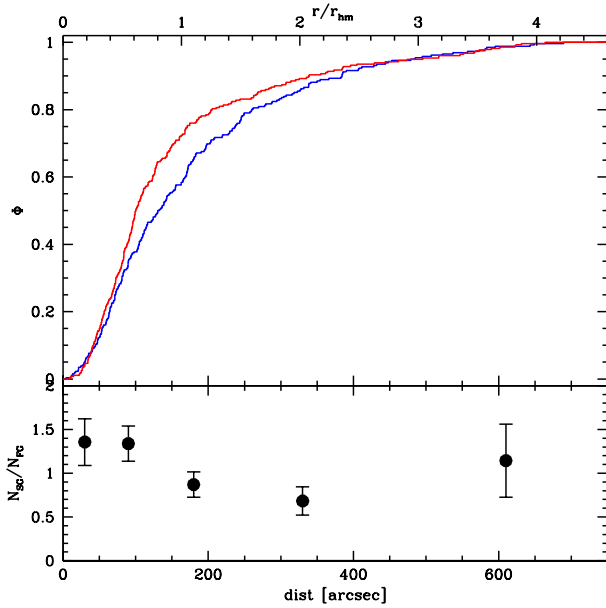


**Figure 7.** *Upper panel:* radial distributions for FG (blue) and SG (red lines) stars. *Lower panel:* SG-to-FG ratio as a function of the distance from the cluster centre. Radial bins are taken within 0.2, 0.6, 1, 2 and 3.5  $r_{hm}$ .

#### 4 SPECTROSCOPIC ANALYSIS

By using Strömgren photometry we have been able to separate two stellar populations in the cluster M3. As already demonstrated in previous works (Carretta et al. 2011b; Sbordone et al. 2011), such a photometric feature indicates that the two populations are characterized by different chemical abundances, in terms of light elements. However, photometry can only give qualitative results in this respect. In order to quantitatively measure the difference in the light element abundances for the two populations we need spectroscopy. Several previous works in the literature studied the chemistry of M3 stars. Therefore we looked for any spectroscopic target with previously measured abundances that has a counterpart in our photometric catalogue, and placed it on our CMD to test our findings.

We retrieved data published by Sneden et al. (2004) and Cohen & Meléndez (2005), but their targets are too bright and they either saturate or are non-linear in our photometry. From the list of Johnson et al. (2005), we found 27 targets that in our photometry are below the non-linearity limit ( $y = 14.1$  mag, anyway fainter than this value the sequences start to mix together) and divided this sample into FG, Na-poor and SG, Na-rich stars depending on their Na abundance with respect to the median<sup>5</sup>  $[Na/Fe]_{med} = -0.07$  dex. Johnson et al. (2005) demonstrate that M3 shows not only the common Na-O anti-correlation, but also that involving Mg and Al, which is not observed in all clusters and tends to be more evident in metal-poor and/or massive GCs (e.g. Carretta et al. 2009b; Cordero et al. 2015). For this reason, we exploited the recently published results of Mészáros et al. (2015), where the authors mea-

sured  $[Al/Fe]$  abundances, and following the same selection criterion we divided their sample into FG, Al-poor and SG, Al-rich stars, depending on each target Al abundance with respect to the median  $[Al/Fe]_{med} = 0.02$  dex. The result of these selection is shown with triangles (Johnson’s targets) and squares (Mészáros’ targets) in Fig.8. Blue symbols represent FG targets, while red symbols show SG ones. RGB stars are marked with filled symbols, while empty symbols highlight likely AGB and HB stars. The spectroscopic separation nicely follows that achieved through photometry. However, despite the good agreement, these targets do not sample the magnitude interval where the photometric separation is more neat. Concerned by this fact, we looked for other targets that could fill such a lack.

We used spectra acquired for a project on RR Lyrae stars in M3 with the multi-object spectrograph FLAMES (Pasquini et al. 2002) at the ESO-VLT (programme 093.D-0536, PI: Contreras Ramos), in a series of 7 exposures of  $\sim 45$  min each with the HR12 setup (5821 - 6146 Å,  $R = 18700$ ), which contains the Na D lines. Since our aim is to spectroscopically confirm whether the two RGB sequences we detected in the CMD of M3 correspond to FG and SG, respectively, we selected only the 17 spectra of the dataset belonging to RGB targets. Since these stars were observed as comparison for HB stars, their magnitude is fainter than for the literature samples and covers the region where the photometric separation is more evident. The data reduction was performed using the dedicated ESO pipeline which includes bias subtraction, flat fielding, wavelength calibration, and spectrum extraction. Individual stellar spectra have been cleaned from sky contribution by subtracting the corresponding median sky spectrum. Finally, multiple spectra of each target have been co-added, reaching a signal-to-noise (S/N) ratio per pixel at about 6000 Å of  $\sim 50$  in the faintest stars and up to 80 in the brightest ones.

After the pre-reduction, we first measured the radial velocities ( $v_r$ ) of each target to determine their membership to the cluster. Radial velocities have been obtained by using DAOSPEC (Stetson & Pancino 2008) and by measuring the position of 34 lines distributed along the whole spectral range covered by the HR12. The uncertainties have been computed as the dispersion of the velocities measured from each line divided by the square root of the number of lines used, and they turned out to be smaller than  $0.4 \text{ km s}^{-1}$ . The heliocentric corrections have been computed with the IRAF task RVCORRECT. All the  $v_r$  measurements and their uncertainties are summarised in Table 2. The mean velocity of the sample turned out to be  $v_r = -148.8 \text{ km s}^{-1}$  ( $\sigma_v = 3.4 \text{ km s}^{-1}$ ), in very good agreement with previous estimates (e.g.  $v_r = -147.6 \text{ km s}^{-1}$ , Harris 1996). Since all of the target velocities lie within  $\pm 3\sigma_v$  from the mean velocity of the cluster (even if we adopt a more robust estimate of  $\sigma_v = 5.6 \text{ km s}^{-1}$ , see McLaughlin & van der Marel 2005) we considered them all as cluster members.

Effective temperatures ( $T_{eff}$ ) and gravities ( $\log g$ ) have been determined photometrically. Since not all of our targets have a counterpart in the Strömgren photometric catalogue (three are missing, see Tab.2), to determine the atmospheric parameters we projected the location of each target in the optical (V, V-I) CMD onto a reference isochrone. This CMD is built from two separated catalogues. One comes from the publicly available HST photometry of Sarajedini et al. 2007 and samples the innermost regions of the cluster, while the other comes from archival MegaCam observations and samples the outer regions. We selected as isochrone an  $\alpha$ -enhanced model with age of 12 Gyr,  $Z = 0.001$  (corresponding to  $[Fe/H] \simeq -1.6$  dex) and standard helium composition re-

<sup>5</sup> This is not what Carretta et al. (2009a,b, 2010b) did. They based the separation between FG and SG on the minimum Na values in their samples of RGB stars, increased by 4 times the uncertainty on Na. However, the samples of stars we are using in the present paper are smaller and the adoption of a median value looks more robust.

trieved from the BaSTI archive (Pietrinferni et al. 2006) and we placed it onto the CMD assuming distance modulus and reddening by Ferraro et al. (1999). The errors associated to these parameters have been computed as described in Massari et al. (2014b), by taking into account the uncertainties on the projection arising from distance modulus ( $\sigma_{DM} = 0.1$  mag), reddening ( $\sigma_{E(B-V)} = 0.05$  mag) and photometry ( $\sigma_V = \sigma_I = 0.02$  mag). They turned out to be of the order of  $\sim 70$  K for  $T_{eff}$  and 0.1 dex for  $\log g$ . Unfortunately, for four targets of our sample we were not able to determine a photometric counterpart, and they have been therefore excluded from the analysis.

The atmospheric parameters were derived by using photometric informations because the limited wavelength range covered by the HR12 does not allow us to use a sufficiently large number of FeI and FeII lines in order to use the fully spectroscopic approach based on the excitation/ionization balance. We used the code GALA<sup>6</sup> (Mucciarelli et al. 2013) to determine the microturbulent velocity ( $v_{turb}$ ) by requiring that no trend exists between iron abundances and line strengths of the lines used, while the photometric temperatures and gravities have been kept fixed during the analysis. For the microturbulent velocity we obtained an average uncertainty of about  $0.2 \text{ km s}^{-1}$ . The atmospheric parameters of the analysed targets are listed in Table 2.

#### 4.1 Elemental abundances

The abundances of iron have been computed by using GALA. The EW and the error of each line were obtained using DAOSPEC, iteratively launched by means of the 4DAO<sup>7</sup> code (Mucciarelli 2013). The lines considered in the analysis have been selected from suitable synthetic spectra at the FLAMES resolution and computed with the SYNTH package (Sbordone et al. 2004) by using the average parameters estimated from photometry and the metallicity derived by Carretta et al. (2009a). The model atmospheres have been computed with the ATLAS9<sup>8</sup> code (Castelli & Kurucz 2004). We adopted the atomic and molecular data from the last release of the Kurucz/Castelli compilation<sup>9</sup> and selected only the lines predicted to be unblended. The final iron abundances of the targets have been computed as the average of each single line measurement, by rejecting all the lines with an EW uncertainty larger than 20%. The errors have been computed by dividing the line-to-line dispersion by the square root of the number of lines used. The average iron abundance for the whole sample of 17 giants is  $[\text{Fe}/\text{H}] = -1.40$  dex ( $\sigma = 0.09$  dex). Such a value is in good agreement with previous estimates like Carretta et al. 2009a or Cavallo & Nagar 2000, which quote  $[\text{Fe}/\text{H}] \simeq -1.5$  dex, and in excellent agreement with Mészáros et al. (2015), who found  $[\text{Fe}/\text{H}] = -1.40$  dex ( $\sigma = 0.08$  dex).

Abundances of NaI have been derived with the spectral synthesis technique performed by using the package SALVADOR (Mucciarelli et al., in prep) from the lines at 5886 and 5892Å. The corresponding internal uncertainties have been computed by means of Monte Carlo simulations. In particular, we added Poissonian noise to the best-fit synthetic spectrum to reproduce the observed SNR and then we repeated the analysis. After 1000 Monte Carlo realizations, the dispersion of the measurements around the mean

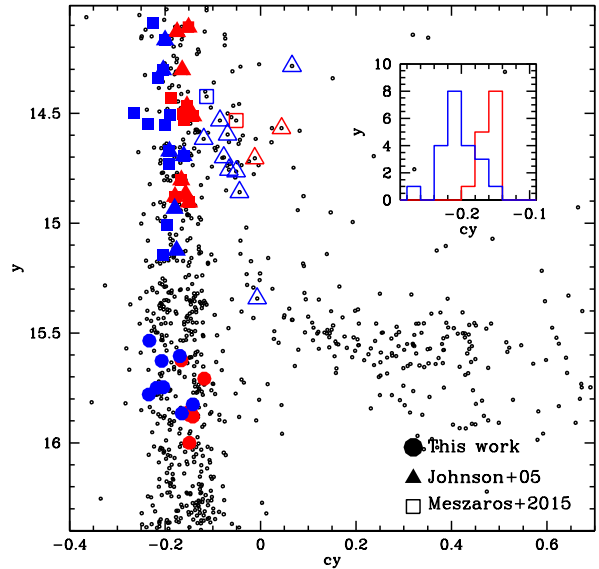


**Figure 8.**  $(y, c_y)$  CMD of M3 zoomed in the RGB region. Targets analysed in this work are highlighted as filled circles (blue ones corresponding to Na-poor, FG stars, red ones to Na-rich, SG), while targets taken from (Johnson et al. 2015a) are marked as filled triangles and those from (Mészáros et al. 2015) as filled squares (with the same colour code). Empty symbols mark non-RGB stars. The inset shows the colour distribution of FG and SG RGB targets, revealing the same bimodality observed photometrically.

value has been adopted as the internal abundance uncertainty. In order to take into account Non Local Thermodynamical Equilibrium (NLTE) effects the abundances derived from the NaI lines have been corrected according to Lind et al. (2011b). The adopted solar reference value have been taken from Grevesse & Sauval (1998). The final values together with the related uncertainties are listed in Table 2.

## 5 RESULTS

Fig.9 shows the numerical distributions of  $[\text{Na}/\text{Fe}]$  with (upper panel) and without (lower panel) correction for NLTE effects. Their dispersions are  $\sigma_{[\text{Na}/\text{Fe}]}^{LTE} = 0.19$  dex and  $\sigma_{[\text{Na}/\text{Fe}]}^{NLTE} = 0.24$  dex, respectively. These values agree well with the finding by Johnson et al. (2005), who found  $\sigma_{[\text{Na}/\text{Fe}]}^{LTE} = 0.25$  dex and  $\sigma_{[\text{Na}/\text{Fe}]}^{NLTE} = 0.26$  dex for a larger sample of 77 stars.

The two distributions do not show a clear-cut bimodality, but only a hint of a separation in two groups. For these reason, we decided to assume the median values of the two distributions to split the sample in Na-poor (FG) and Na-rich (SG) stars, as done for the stars retrieved from the sample of Mészáros et al. (2015). Median values are shown in Fig.9 with vertical red dashed lines. We cross-correlated the spectroscopic targets with our photometric catalogue, finding 14 matches (targets IDs, coordinates and magnitudes are listed in Tab.2, where  $ID_{spec}$  corresponds to that used in the spectroscopic archive and  $ID_{phot}$  to that used in our photometric catalogue.). Their location in the Strömbergren  $(y, c_y)$  CMD is shown with filled blue (FG) and red (SG) circles in Fig.8.

The position of the targets follows quite well the bimodality of

<sup>6</sup> <http://www.cosmic-lab.eu/gala/gala.php>

<sup>7</sup> <http://www.cosmic-lab.eu/4dao/4dao.php>

<sup>8</sup> <http://wwwuser.oats.inaf.it/castelli/sources/atlas9codes.html>

<sup>9</sup> <http://wwwuser.oats.inaf.it/castelli/linelists.html>

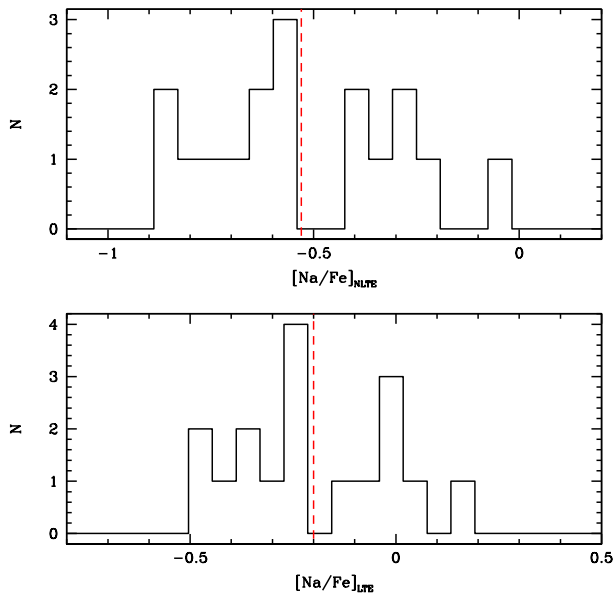


**Figure 9.** Histograms of the  $[\text{Na}/\text{Fe}]$  distributions of our analysed targets before (*lower panel*) and after (*upper panel*) NLTE corrections. The median values of the two distributions are also marked with the two vertical red dashed lines.

the RGB detected photometrically, with all the Na-rich stars located on the right RGB, and the majority of Na-poor stars distributed along the left RGB, with only few outliers.

In order to highlight the nice separation of all the spectroscopic FG and SG targets, we show their colour distribution in the inset of the Figure. Two main peaks appear to be very well defined, and this appearance is confirmed by both the GMM test and the dip-test, which confirm the bimodality of the distribution with a statistical significance larger than 99.9%. A further confirmation of the good correspondence between our photometric and spectroscopic results comes from the number-ratio of the two populations. In fact, from our spectroscopic sample we found that FG and SG are equal in number within the Poissonian uncertainty, with the FG accounting for the  $56 \pm 8\%$  against the  $44 \pm 11\%$  of SG stars. This result is in good agreement with our photometric estimate ( $48 \pm 3\%$  of FG and  $52 \pm 3\%$  of SG members, see Sect.3). It is also worth noticing that among the 12 AGB targets found in the literature samples, the number ratio of the two population is significantly different from that measured in our sample along the RGB. In fact, nine stars appear to belong to the FG and the remaining three to the SG, this leading to a 75%-25% ratio. Such a finding is interesting because it represents one of the few measurement in the disputed topic concerning the behaviour of GC multiple generations along the AGB. In fact, recently a few metal-poor GCs were found to show no SG-AGB stars at all. This is the case for NGC 6752 (Campbell et al. 2013) and for M62 (Lapenna et al. 2015), though in the latter case the lack of SG-AGB stars is possibly due to the small sample of studied stars. However, in several other cases (Johnson et al. 2015b; García-Hernández et al. 2015) SG-AGB stars have indeed been detected. M3 belongs to the second of these groups, since García-Hernández et al. (2015) already found three SG-AGB stars using APOGEE spectra. In this work we confirm this finding and we add other three of such rare targets.

## 6 SUMMARY AND CONCLUSIONS

In this work, we exploited a ground based photometric dataset in Strömgren *uvby* filters to study the multiple stellar generations of the GC M3. The analysis of the CMD built with the  $c_y$  index has shown the presence of a double RGB, equally populated in its two components. The radial distributions of the two populations turned out to be quite peculiar, with red and blue sequence being completely mixed up to about the half-mass radius, then changing the observed trend with the red component staying more centrally concentrated out to about  $\sim 3.5 r_{hm}$ , when the two mix again. Such a trend is predicted to be observed in clusters which experienced moderate dynamical evolution, and it confirms previous dynamical age estimate available in literature.

The spectroscopic analysis of a sample of 17 giants observed with FLAMES, and the comparison with previous abundance measurements available in literature, demonstrated that the photometric detection of the two RGBs flags the presence of chemically distinct populations with the FG corresponding to the left sequence and the SG to the right, as observed in all the other metal-poor and metal-intermediate clusters studied so far with the Strömgren  $c_y$  index. We also found three new SG-AGB stars, thus confirming that the lack of such stars observed in other metal-poor GCs is not an ubiquitous feature.

Our work therefore demonstrates yet again how efficient Strömgren photometry is to study the phenomenon of multiple stellar generations in GCs over the large field of view and the large number of samples stars permitted by ground-based photometric observations and how important is to couple spectroscopic and photometric information to characterise globular cluster populations.

## ACKNOWLEDGEMENTS

We thank the referee Judith Cohen for her report and suggestions which helped us to improve the presentation of our results. This paper makes use of data obtained from the Isaac Newton Group Archive which is maintained as part of the CASU Astronomical Data Centre at the Institute of Astronomy, Cambridge. This paper also uses observations made with ESO Telescopes at the La Silla Paranal Observatory under programme ID 093.D-0536. DM has been supported by the FIRB 2013 (MIUR grant RBFR13J716). EL and ED have been supported by COSMIC-LAB (web site: <http://www.cosmic-lab.eu>), which is funded by the European Research Council (under contract ERC-2010-AdG-267675). AB acknowledges partial support from PRIN-MIUR 2010-2011 The Chemical and Dynamical Evolution of the Milky Way and Local Group Galaxies (PI F. Matteucci). PA acknowledges Proyecto Fondecyt Regular 1150345. This research made use of the SIMBAD database, operated at CDS, Strasbourg, France and of NASAs Astrophysical Data System.



**Table 2.** Photometric and spectroscopic quantities of the analysed targets.

ID <sub>spec</sub>	ID <sub>phot</sub>	R.A.	Dec.	u	v	b	y	v <sub>r</sub>	T <sub>eff</sub>	log g	v <sub>turb</sub>	[Fe/H]	[Na/H] <sub>LTE</sub>	[Na/H] <sub>NLTE</sub>
		(J2000)	(J2000)	mag	mag	mag	mag	km s <sup>-1</sup>	K	dex	km s <sup>-1</sup>	dex	dex	dex
100579	1986	205.6562914	28.4329251	16.592	15.077	13.950	13.602	-151.9 ± 0.3	5068	2.5	1.85	-1.42 ± 0.09	-1.42 ± 0.08	-1.72 ± 0.17
103981	6897	205.6844581	28.3859233	16.378	14.828	13.644	13.265	-148.7 ± 0.3	5019	2.4	2.05	-1.32 ± 0.10	-1.58 ± 0.03	-1.91 ± 0.10
18711	1185	205.3888267	28.4484213	16.527	15.017	13.861	13.555	-149.1 ± 0.3	5060	2.5	2.05	-1.43 ± 0.13	-1.66 ± 0.02	-2.01 ± 0.07
25241	13795	205.4358151	28.3377528	16.607	15.074	13.945	13.584	-147.0 ± 0.2	5060	2.5	1.60	-1.29 ± 0.11	-1.41 ± 0.06	-1.69 ± 0.15
27510	4189	205.4475563	28.4100074	16.565	15.068	13.875	13.596	-151.9 ± 0.4	5068	2.5	1.90	-1.27 ± 0.07	-1.68 ± 0.09	-2.04 ± 0.18
42796	7302	205.5012666	28.3856410	16.462	14.985	13.796	13.480	-152.1 ± 0.3	5043	2.4	2.30	-1.37 ± 0.10	-1.70 ± 0.04	-2.08 ± 0.12
48341	3543	205.5150179	28.4149743	16.432	14.993	13.812	13.510	-146.4 ± 0.3	5042	2.4	1.65	-1.40 ± 0.07	-1.65 ± 0.04	-2.01 ± 0.12
53478	2477	205.5264945	28.4280449	16.378	14.846	13.650	13.335	-147.9 ± 0.4	5012	2.4	1.90	-1.44 ± 0.12	-1.72 ± 0.04	-2.08 ± 0.13
53570	14330	205.5267239	28.3307889	16.382	14.856	13.707	13.354	-148.0 ± 0.2	5011	2.3	1.85	-1.41 ± 0.09	-1.50 ± 0.05	-1.82 ± 0.14
67305	12304	205.5563429	28.3497774	16.486	14.926	13.783	13.438	-148.2 ± 0.3	5020	2.4	2.00	-1.43 ± 0.12	-1.40 ± 0.04	-1.68 ± 0.13
78766	2615	205.5813052	28.4254582	16.663	15.176	14.040	13.730	-148.0 ± 0.3	5081	2.5	1.85	-1.42 ± 0.08	-1.41 ± 0.08	-1.70 ± 0.17
95001	229	205.6299793	28.4645877	16.311	14.901	13.815	13.477	-148.1 ± 0.4	5043	2.4	1.95	-1.70 ± 0.11	-2.08 ± 0.16	-2.50 ± 0.19
96900	8553	205.6379019	28.3754247	16.578	15.070	13.949	13.610	-140.3 ± 0.3	5057	2.5	2.05	-1.42 ± 0.10	-1.25 ± 0.04	-1.49 ± 0.11
97013	15559	205.6383057	28.3134164	16.328	14.851	13.716	13.357	-150.5 ± 0.2	5013	2.4	1.60	-1.35 ± 0.12	-1.81 ± 0.02	-2.20 ± 0.06
104765	-	-	-	-	-	-	-	-157.5 ± 0.5	5023	2.4	1.90	-1.41 ± 0.10	-1.87 ± 0.08	-2.28 ± 0.15
28686	-	-	-	-	-	-	-	-148.5 ± 0.3	5048	2.4	1.95	-1.45 ± 0.09	-1.46 ± 0.03	-1.77 ± 0.08
69664	-	-	-	-	-	-	-	-149.0 ± 0.2	5073	2.5	1.50	-1.33 ± 0.07	-1.58 ± 0.05	-1.92 ± 0.10

## REFERENCES

- Anthony-Twarog B. J., Twarog B. A., Craig J., 1995, *PASP*, 107, 32
- Árnadóttir A. S., Feltzing S., Lundström I., 2010, *A&A*, 521, A40
- Bastian N., Lamers H. J. G. L. M., de Mink S. E., Longmore S. N., Goodwin S. P., Gieles M., 2013, *MNRAS*, 436, 2398
- Bastian N., Cabrera-Ziri I., Salaris M., 2015a, *MNRAS*, 449, 3333
- Bastian N., Cabrera-Ziri I., Salaris M., 2015b, *MNRAS*, 449, 3333
- Beccari G., Bellazzini M., Lardo C., Bragaglia A., Carretta E., Dalessandro E., Mucciarelli A., Pancino E., 2013, *MNRAS*, 431, 1995
- Bedin L. R., Piotto G., Anderson J., Cassisi S., King I. R., Momany Y., Carraro G., 2004, *ApJ*, 605, L125
- Bragaglia A., et al., 2010, *ApJ*, 720, L41
- Bragaglia A., Carretta E., Sollima A., Donati P., D’Orazi V., Gratton R. G., Lucatello S., Sneden C., 2015, *A&A*, 583, A69
- Calamida A., et al., 2007, *ApJ*, 670, 400
- Campbell S. W., et al., 2013, *Natur*, 498, 198
- Castelli F., Kurucz R. L., 2004, *astro*, arXiv:astro-ph/0405087
- Carretta E., Bragaglia A., Gratton R., Lucatello S., 2009b, *A&A*, 505, 139
- Carretta E., et al., 2009a, *A&A*, 505, 117
- Carretta E., et al., 2010b, *ApJ*, 714, L7
- Carretta E., Lucatello S., Gratton R. G., Bragaglia A., D’Orazi V., 2011, *A&A*, 533, A69
- Carretta E., Bragaglia A., Gratton R., D’Orazi V., Lucatello S., 2011, *A&A*, 535, A121
- Carretta E., Bragaglia A., Gratton R. G., D’Orazi V., Lucatello S., Sollima A., 2014, *A&A*, 561, A87
- Carretta E., 2015, *ApJ*, 810, 148
- Cavallo R. M., Nagar N. M., 2000, *AJ*, 120, 1364
- Cohen J. G., 2004, *AJ*, 127, 1545
- Cohen J. G., Meléndez J., 2005, *AJ*, 129, 303
- Cordero M. J., Pilachowski C. A., Johnson C. I., Vesperini E., 2015, *ApJ*, 800, 3
- D’Antona F., Bellazzini M., Caloi V., Fusi Pecci F., Galleti S., Rood R. T., 2005, *ApJ*, 631, 868
- D’Ercole A., Vesperini E., D’Antona F., McMillan S. L. W., Recchi S., 2008, *MNRAS*, 391, 825
- Dalessandro E., Salaris M., Ferraro F. R., Cassisi S., Lanzoni B., Rood R. T., Fusi Pecci F., Sabbi E., 2011, *MNRAS*, 410, 694
- Dalessandro E., Salaris M., Ferraro F. R., Mucciarelli A., Cassisi S., 2013, *MNRAS*, 430, 459
- Dalessandro E., et al., 2014, *ApJ*, 791, L4
- Decressin T., Meynet G., Charbonnel C., Prantzos N., Ekström S., 2007, *A&A*, 464, 1029
- Dupree A. K., Avrett E. H., 2013, *ApJ*, 773, L28
- Ferraro F. R., Messineo M., Fusi Pecci F., de Palo M. A., Straniero O., Chieffi A., Limongi M., 1999, *AJ*, 118, 1738
- Ferraro F. R., et al., 2009, *Natur*, 462, 483
- Ferraro F. R., et al., 2012, *Natur*, 492, 393
- Frank M. J., Koch A., Feltzing S., Kacharov N., Wilkinson M. I., Irwin M., 2015, *A&A*, 581, A72
- García-Hernández D. A., Mészáros S., Monelli M., Cassisi S., Stetson P. B., Zamora O., Shetrone M., Lucatello S., 2015, *ApJ*, 815, L4
- Gratton R. G., D’Orazi V., Bragaglia A., Carretta E., Lucatello S., 2010, *A&A*, 522, A77
- Gratton R. G., Carretta E., Bragaglia A., 2012, *A&ARv*, 20, 50
- Grevesse N., Sauval A. J., 1998, *SSRv*, 85, 161
- Grundahl F., VandenBerg D. A., Andersen M. I., 1998, *ApJ*, 500, L179
- Grundahl F., Catelan M., Landsman W. B., Stetson P. B., Andersen M. I., 1999, *ApJ*, 524, 242
- Han S.-I., Lee Y.-W., Joo S.-J., Sohn S. T., Yoon S.-J., Kim H.-S., Lee J.-W., 2009, *ApJ*, 707, L190
- Harris W. E., 1996, *AJ*, 112, 1487
- Henault-Brunet V., 2015, *IAUGA*, 22, 2252802
- Ivans I. I., Sneden C., Gallino R., Cowan J. J., Preston G. W., 2005, *ApJ*, 627, L145
- Johnson C. I., Kraft R. P., Pilachowski C. A., Sneden C., Ivans I. I., Benman G., 2005, *PASP*, 117, 1308
- Johnson C. I., Pilachowski C. A., 2010, *ApJ*, 722, 1373
- Johnson C. I., Rich R. M., Pilachowski C. A., Caldwell N., Mateo M., Bailey J. I., III, Crane J. D., 2015, *AJ*, 150, 63
- Johnson C. I., et al., 2015, *AJ*, 149, 71
- Lapenna E., Mucciarelli A., Lanzoni B., Ferraro F. R., Dalessandro E., Origlia L., Massari D., 2014, *ApJ*, 797, 124
- Lapenna E., Mucciarelli A., Ferraro F. R., Origlia L., Lanzoni B., Massari D., Dalessandro E., 2015, *ApJ*, 813, 97
- Lardo C., Bellazzini M., Pancino E., Carretta E., Bragaglia A., Dalessandro E., 2011, *A&A*, 525, A114
- Lardo C., Mucciarelli A., Bastian N., 2016, *MNRAS*, 457, 51
- Larsen S. S., Baumgardt H., Bastian N., Brodie J. P., Grundahl F., Strader J., 2015, *ApJ*, 804, 71
- Lee Y.-W., Joo J.-M., Sohn Y.-J., Rey S.-C., Lee H.-C., Walker A. R., 1999, *Natur*, 402, 55
- Lind K., Asplund M., Barklem P. S., Belyaev A. K., 2011, *A&A*, 528, A103
- Lind K., Charbonnel C., Decressin T., Primas F., Grundahl F., Asplund M., 2011a, *A&A*, 527, A148
- Marino A. F., et al., 2011a, *A&A*, 532, A8
- Marino A. F., et al., 2011b, *ApJ*, 731, 64
- Marino A. F., et al., 2015, *MNRAS*, 450, 815
- Massari D., et al., 2014, *ApJ*, 795, 22
- Massari D., et al., 2014, *ApJ*, 791, 101
- Massari D., et al., 2016, *A&A*, 586, A51
- McLaughlin D. E., van der Marel R. P., 2005, *ApJS*, 161, 304
- Mészáros S., et al., 2015, *AJ*, 149, 153
- Miholics M., Webb J. J., Sills A., 2015, *MNRAS*, 454, 2166
- Milone A. P., et al., 2012, *ApJ*, 744, 58
- Milone A. P., et al., 2015a, *MNRAS*, 447, 927
- Milone A. P., et al., 2015b, *ApJ*, 808, 51
- Miocchi P., et al., 2013, *ApJ*, 774, 151
- Monelli M., et al., 2013, *MNRAS*, 431, 2126
- Mucciarelli A., 2013, arXiv, arXiv:1311.1403
- Mucciarelli A., Pancino E., Lovisi L., Ferraro F. R., Lapenna E., 2013, *ApJ*, 766, 78
- Mucciarelli A., Lapenna E., Massari D., Pancino E., Stetson P. B., Ferraro F. R., Lanzoni B., Lardo C., 2015, *ApJ*, 809, 128
- Mucciarelli A., Lapenna E., Massari D., Ferraro F. R., Lanzoni B., 2015, *ApJ*, 801, 69
- Muratov A. L., Gnedin O. Y., 2010, *ApJ*, 718, 1266
- Nardiello D., Milone A. P., Piotto G., Marino A. F., Bellini A., Cassisi S., 2015, *A&A*, 573, A70
- Norris J. E., Da Costa G. S., 1995, *ApJ*, 447, 680
- Origlia L., et al., 2011, *ApJ*, 726, L20
- Origlia L., Massari D., Rich R. M., et al. 2013, *ApJ*, 799, L5 (O13)
- Pasquini L., et al., 2002, *Msngr*, 110, 1
- Pasquini L., Mauas P., Käuff H. U., Cacciari C., 2011, *A&A*, 531, A35
- Paunzen E., 2015, *A&A*, 580, A23
- Pietrinferni A., Cassisi S., Salaris M., Castelli F., 2006, *ApJ*, 642, 797
- Piotto G., et al., 2002, *A&A*, 391, 945
- Piotto G., et al., 2005, *ApJ*, 621, 777
- Piotto G., et al., 2007, *ApJ*, 661, L53
- Piotto G., et al., 2015, *AJ*, 149, 91
- Renzini A., Buzzoni A., 1986, *ASSL*, 122, 195
- Renzini A., et al., 2015, *MNRAS*, 454, 4197
- Richter P., Hilker M., Richtler T., 1999, *A&A*, 350, 476
- Roederer I. U., Mateo M., Bailey J. I., III, Spencer M., Crane J. D., Shectman S. A., 2015, arXiv, arXiv:1510.06414
- Roh D.-G., Lee Y.-W., Joo S.-J., Han S.-I., Sohn Y.-J., Lee J.-W., 2011, *ApJ*, 733, L45
- Salaris M., Cassisi S., 2014, *A&A*, 566, A109
- Sarajedini A., et al., 2007, *AJ*, 133, 1658
- Sbordone L., Bonifacio P., Castelli F., Kurucz R. L., 2004, *MSAIS*, 5, 93
- Sbordone L., Salaris M., Weiss A., Cassisi S., 2011, *A&A*, 534, A9
- Skrutskie M. F., et al., 2006, *AJ*, 131, 1163
- Sneden C., Kraft R. P., Guhathakurta P., Peterson R. C., Fulbright J. P., 2004, *AJ*, 127, 2162
- Stetson P. B., Pancino E., 2008, *PASP*, 120, 1332

- Stetson P. B., 1994, *PASP*, 106, 250  
Stetson P. B., 1987, *PASP*, 99, 191  
Tautvaišienė G., Wallerstein G., Geisler D., Gonzalez G., Charbonnel C., 2004, *AJ*, 127, 373  
Valcarce A. A. R., Catelan M., Alonso-García J., Contreras Ramos R., Alves S., 2016, arXiv, arXiv:1601.06747  
VandenBerg, D. A., Brogaard, K., Leaman, R., & Casagrande, L. 2013, *ApJ*, 775, 134  
Vesperini E., McMillan S. L. W., D'Antona F., D'Ercole A., 2013, *MNRAS*, 429, 1913  
Villanova S., Geisler D., Carraro G., Moni Bidin C., Muñoz C., 2013, *ApJ*, 778, 186  
Yong D., Grundahl F., 2008, *ApJ*, 672, L29  
Yong D., Grundahl F., Johnson J. A., Asplund M., 2008, *ApJ*, 684, 1159  
Yong D., et al., 2014, *MNRAS*, 441, 3396

This paper has been typeset from a  $\text{\TeX}/\text{\LaTeX}$  file prepared by the author.